iScience

Article

# Hepatic Lamp2a deficiency promotes inflammation of murine autoimmune cholangitis via affecting bile acid metabolism

## Graphical abstract

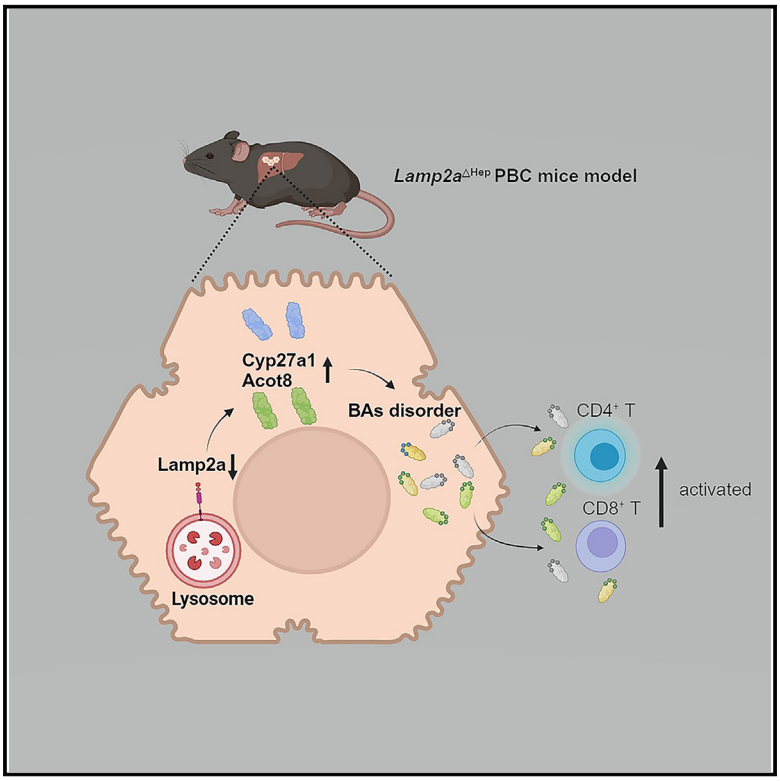


## Authors

Qingling Fan, Guanya Guo, Yinan Hu, ..., Jingbo Wang, Ting Li, Ying Han

## Correspondence

jimberw@163.com (J.W.), tinglilt18@fmmu.edu.cn (T.L.), hanying1@fmmu.edu.cn (Y.H.)

## In brief

Immunology; Transcriptomics

## Highlights

- Hepatic-specific Lamp2a deficiency promotes murine autoimmune cholangitis
- Loss of hepatic Lamp2a enhance T cell activation by disturbing bile acids metabolism
- Acot8 knockdown alleviates the liver inflammation caused by Lamp2a deficiency

Fan et al., 2025, iScience *28*, 111804
February 21, 2025 
https://doi.org/10.1016/j.isci.2025.111804

CellPress

iScience

CellPress
OPEN ACCESS

Article

# Hepatic Lamp2a deficiency promotes inflammation of murine autoimmune cholangitis via affecting bile acid metabolism

Qingling Fan,[1,2] Guanya Guo,[1,2] Yinan Hu,[1] Yi Lu,[1] Rui Su,[1] Jiaqi Yang,[1] Erzhuo Xia,[1] Shuoyi Ma,[1] Miao Zhang,[1] Jingbo Wang,[1,*] Ting Li,[1,*] and Ying Han[1,3,*]

[1]Xijing Hospital of Digestive Diseases, State Key Laboratory of Holistic Integrative Management of Gastrointestinal Cancers, Air Force Medical University, Xi'an 710032, China

[2]These authors contributed equally

[3]Lead contact

*Correspondence: jimberw@163.com (J.W.), tinglilt18@fmmu.edu.cn (T.L.), hanying1@fmmu.edu.cn (Y.H.)

https://doi.org/10.1016/j.isci.2025.111804

## SUMMARY

Primary biliary cholangitis is characterized by breaking of immune tolerance and disorders of bile acid metabolism. Our previous study found that abnormal expression of Lamp2 was detected in PBC patients. However, the specific role of Lamp2a in disease progression is still unclear. In this study, we showed that hepatic-specific Lamp2a deficiency could aggravate the inflammatory phenotype of murine autoimmune cholangitis. Mechanistically, the loss of Lamp2a in hepatocytes contributed to the abnormal accumulation of Acot8, thus altered the bile acid components, thereby enhancing the lymphocyte activities, and ultimately promoting the inflammatory phenotype of model mice. Moreover, we also found that Acot8 knockdown could alleviate the liver inflammation caused by Lamp2a deficiency. Altogether, our findings explored the effect of Lamp2a deficiency on the murine autoimmune cholangitis by the perspective of bile acid metabolism, and marked the possibility of Acot8 as a new target for the treatment of PBC disease.

## INTRODUCTION

Primary biliary cholangitis (PBC) is a chronic cholestatic autoimmune liver disease characterized by positive-antimitochondrial antibodies and abnormal liver function, including elevated γ-glutamyltransferase (GGT) or alkaline phosphatase (ALP).[1–5] While the pathogenesis is still unclarified, studies have shown that the breaking of immune tolerance in PBC patients is closely associated with the disorders of bile acid metabolism, which has become an important indicator in PBC diagnosis and prognosis evaluation.[6–11] Correction of bile acid metabolism disorders can effectively relieve the symptoms of PBC.[11,12] Ursodeoxycholic acid (UDCA) is a Food and Drug Administration (FDA) approved first-line treatment for PBC, and many other bile acid analogs have also shown promising therapeutic prospects.[11,13–15] Therefore, it has important theoretical and practical significance to explore the pathogenesis of PBC from the perspective of bile acid metabolism for deep understanding of disease progression and targeted treatment.

Autophagy is essential to the recycling of cellular material and is involved in the post-translational regulation of proteins.[16,17] Impaired autophagy has been detected in several cholestatic liver diseases, including PBC, in the form of increased LC3 and p62.[18–21] Lysosome-associated membrane protein-2 (Lamp2) is a key regulatory molecule of autophagy.[22,23] Our previous study found that the absence of Lamp2 exacerbated the cholestasis and elevated serum ALP in the rat bile duct ligation (BDL) model, which are also important clinical features of PBC.[24] Moreover, we also found that increased serum Lamp2 levels in PBC patients could reflect the efficacy of UDCA.[25] We identified and demonstrated the elevated expression and redistribution of Lamp2 in the liver of PBC patients.[26] Interestingly, the subcellular localization of Lamp2 was also redistributed. These findings suggest that Lamp2 plays an important role during disease progression. Lamp2 is a critical marker of intracellular autophagy, and the changes of its expression and distribution imply a disturbance of autophagy function. Alternative splicing of the Lamp2 gene produces three variants: LAMP2A, LAMP2B, and LAMP2C, which are involved in different types of autophagy regulation respectively.[27–32] LAMP2A is the receptor for chaperone-mediated autophagy (CMA), and highly expressed in hepatocytes.[29] As a substrate of the CMA pathway, the level of the bile acid metabolism enzyme CYP27a1 remained unchanged,[33] suggesting that the Increased Lamp2 could be nonfunctional. Our recent study showed that elevated level of Lamp2a in $CD4^+$ T cells is associated with its hyperactivity in PBC patients.[28,34] However, how hepatic Lamp2a affects the disease progression of PBC remains to be investigated.[35–37] Based on these, we used Lamp2a knockout mice in this study to address the role of autophagy disorders in PBC model.

Several acyl-CoA thioesterases (Acots), including Acot8, participate in bile acid biosynthesis that catalyze the hydrolysis

of bile acid-CoAs to the free bile acid and coenzyme A.[37] Previous studies have shown that Acot8 has a broad tissue expression in mice and human, and plays a role in the regulation of fatty acid oxidation.[38,39] Although studies about the interaction between Lamp2a and Acot8 have not been reported yet, using the online website KFERQ finder V0.8, we found the pentapeptide motif of KFERQ as the Lamp2a substrate in the amino acid sequence of Acot8, suggesting that Acot8 may be degraded through the CMA pathway. Nevertheless, how Lamp2a participates in PBC disease progression through regulating Acot8 has not been elucidated. In this study, we describe the role of hepatic-specific Lamp2a affecting murine autoimmune cholangitis by regulating bile acid metabolism, hoping to provide theoretical and experimental basis for new targets of PBC therapy.

## RESULTS

### Hepatic-specific Lamp2a deficiency aggravates the liver inflammatory response of murine autoimmune cholangitis

Our previous study suggested that the absence of Lamp2 exacerbated the cholestasis and elevated serum ALP in the rat BDL model. To explore the role of Lamp2a in the murine autoimmune cholangitis, we employed representative models of transgenic or immunized for this study, which are dnTGF-βRII mice and 2OA-BSA immunized mice (Figure S1A), respectively. Here, the levels of Lamp2a in mouse autoimmune cholangitis models were examined. Remarkably, both models exhibited an inflammatory infiltration of the liver, structural disruption of the small bile ducts, and elevated biochemical index (Figures S1B–S1G). Importantly, we found that both the mRNA and the protein levels of Lamp2a were decreased in dnTGF-βRII ($Tg^+$) mice (Figures S1H and S1I), while upon the 2-OA induction, the hepatic Lamp2a levels showed no obvious change (Figures S1J and S1K). The two models showed different trends in Lamp2a levels could be because they were built on disparate principle. Whether Lamp2a plays a role in PBC progression needs further exploration.

To establish the cell-specific role of Lamp2a in hepatocytes, we generated hepatic-specific Lamp2a deficiency mice ($Lamp2a^{\Delta Hep}$) by crossing $Lamp2a^{flox/flox}$ mice with Alb-Cre mice, which did not affect the immune status of the liver (Figure S2). To explore the role of Lamp2a during PBC progression, we either crossed $Lamp2a^{\Delta Hep}$ mice with dnTGF-βRII mice (Figures S3A–S3C) or treated the $Lamp2a^{\Delta Hep}$ mice with 2OA (Figures S3A and S3D). As shown, the loss of hepatic Lamp2a resulted in more severe lymphocytic infiltration, especially around the bile duct of the liver in both models (Figures 1A–1C). Not only increased the abundance of $CD4^+$ and $CD8^+$ T cells, the activation percentages and cytotoxicity of $CD8^+$ T cells, marked as the ratio of $CD44^{high}$ to $CD8^+$ T cells and IFN-$\gamma^+$ of $CD8^+$ T cells, respectively, were also significantly heightened (Figures 1D and S3E). Although no significant difference was observed in the destruction of bile duct structure and fibrosis (Figures 1E and S3F), we detected an increased ductular reaction by CK19 staining (Figure 1B) and higher levels of secreted inflammatory cytokines in the Lamp2a deficiency models (Figure 1F). In addition, the serological index of the liver did not change significantly in both transgenic and immunized models (Figure S3G). The data aforementioned indicate that hepatic-specific Lamp2a deficiency promotes liver inflammatory response of murine autoimmune cholangitis.

### Hepatocyte Lamp2a rescue could alleviate the progression of murine autoimmune cholangitis

To further confirm the role of Lamp2a in promoting hepatic inflammatory infiltration, we intravenously injected Adeno-associated virus carrying Lamp2a expression plasmid into $Lamp2a^{\Delta Hep}Tg^+$ mice (Figures 2A and 2B). Compared with mice injected with control virus, re-expression of Lamp2a alleviated inflammatory infiltration in the liver (Figures 2C–2E) and T cell activation were also reduced (Figures 2F and S4A). And the rescue of Lamp2a led to an improvement in liver function (Figure 2G), while the levels of the inflammatory cytokines did not change significantly (Figure 2H). Moreover, the re-expression of Lamp2a showed the same trend in the 2OA model (Figures S4B–S4D). Additionally, extrinsic Lamp2a expression in $Lamp2a^{fl/fl}Tg^+$ mice made no change in hepatic inflammation (Figures S4E–S4G). Taken together, these results indicate that the rescue of Lamp2a alleviates the hepatic inflammatory phenotype in both model mice, which confirm the important role of Lamp2a in murine autoimmune cholangitis.

### Hepatic-specific Lamp2a deficiency affects bile acid metabolism

As we mentioned earlier, the deregulation of bile acid metabolism plays a critical role in the disease development of PBC. To study the actual effect of Lamp2a on the component of bile acid metabolism, we performed bile acid metabolomic study in the livers of both PBC model mice. As shown in Figure 3A, we detected 1 significant upregulate bile acid and 2 downregulated bile acids in $Lamp2a^{\Delta Hep}$ $Tg^+$ mice compared with the control $Lamp2a^{fl/fl}Tg^+$ mice. On the other hand, we found 9 upregulated bile acids $Lamp2a^{\Delta Hep}$ -2OA group compared with the control $Lamp2a^{fl/fl}$-2OA mice. Comparing the two sets of omics results, we found that six bile acids, 6-keto lithocholic acid (6-KetoLCA), hyodeoxycholic acid (HDCA), dehydrocholic acid (7-DHCA), lithocholic acid (LCA), deoxycholic acid (DCA), and chenodeoxycholic acid (CDCA), showed elevated trends in Lamp2a hepatic-deficient mice in both models (Figures 3B and 3C). Similarly, compare with the $Lamp2a^{fl/fl}$ mice, several of these bile acids also showed an elevation in the liver of $Lamp2a^{\Delta Hep}$ mice (Figure S5A). We found HDCA and CDCA concentrations accordingly decreased after Lamp2a rescue (Figure S5B), suggesting that these bile acids, especially HDCA and CDCA, might be the key factors causing the aggravation of liver inflammation, which will be further explored in subsequent studies.

### Bile acid-metabolizing enzyme Acot8 is degraded by CMA mediated by Lamp2a

To further determine the specific mechanism by which Lamp2a deficiency affects the bile acid metabolism pathways, we extracted RNA and protein samples from $Lamp2a^{\Delta Hep}Tg^+$ and $Lamp2a^{fl/fl}Tg^+$ mice, and performed quantitative RNA sequencing on $Lamp2a^{\Delta Hep}Tg^+$ and $Lamp2a^{fl/fl}Tg^+$ mice. The mRNA expression of enzymes involved in bile acid synthesis

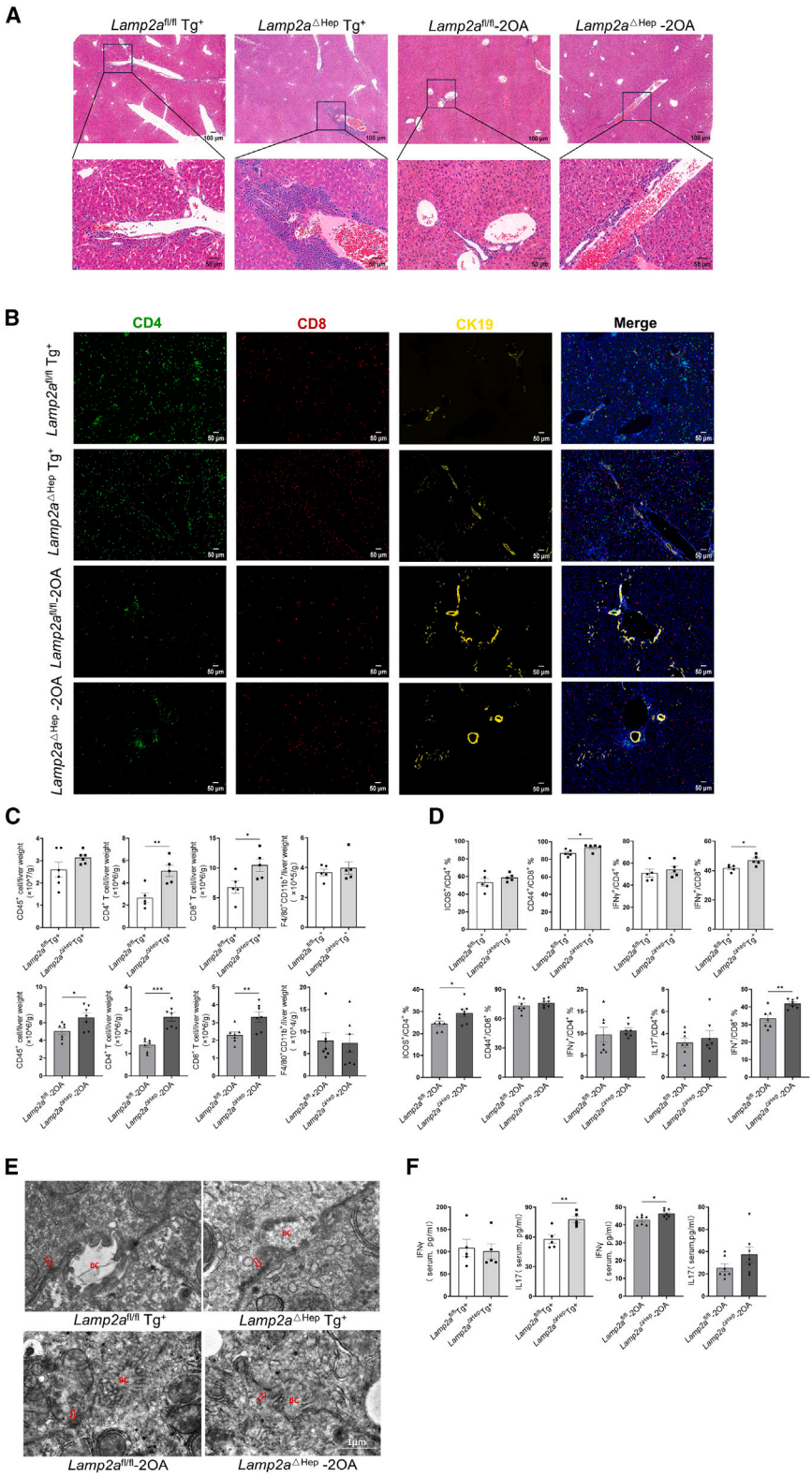


**Figure 1. Hepatic Lamp2a knockout aggravates liver inflammation in PBC mice models**

(A) H&E staining of liver section from the *Lamp2a*$^{fl/fl}$Tg$^{+}$, *Lamp2a*$^{\Delta Hep}$ Tg$^{+}$, *Lamp2a*$^{fl/fl}$-2OA, and *Lamp2a*$^{\Delta Hep}$ -2OA groups. (Tg$^{+}$ model, $n = 5$ mice per group; 2OA models $n = 7$ mice per group; scale bar labeled in the figure).

(B) CD4(green), CD8(red), and CK19(yellow) IF staining of liver section described in a. (scale bar labeled in the figure).

(C) Percentages of CD45.2$^{+}$, CD4$^{+}$ CD8$^{+}$, and CD11b$^{+}$ F4/80$^{+}$ cells in livers described in a, as determined by flow cytometry.

(*, $p < 0.05$; **, $p < 0.01$; ***, $p < 0.005$).

(D) Percentages of the indicated leukocyte subsets in livers described in (A), as determined by flow cytometry.

(*, $p < 0.05$; **, $p < 0.01$).

(E) Electron microscopic examination of the bile canaliculi in livers of from mice described in (A). (scale bar labeled in the figure).

(F) IFN-γ and IL17 levels in serum from mice described in a, determined by ELISA. ($n = 5$ mice per group; *, $p < 0.05$; **, $p < 0.01$). Statistical significance was determined by two-tailed unpaired t test. Data are presented as means ± SEM.

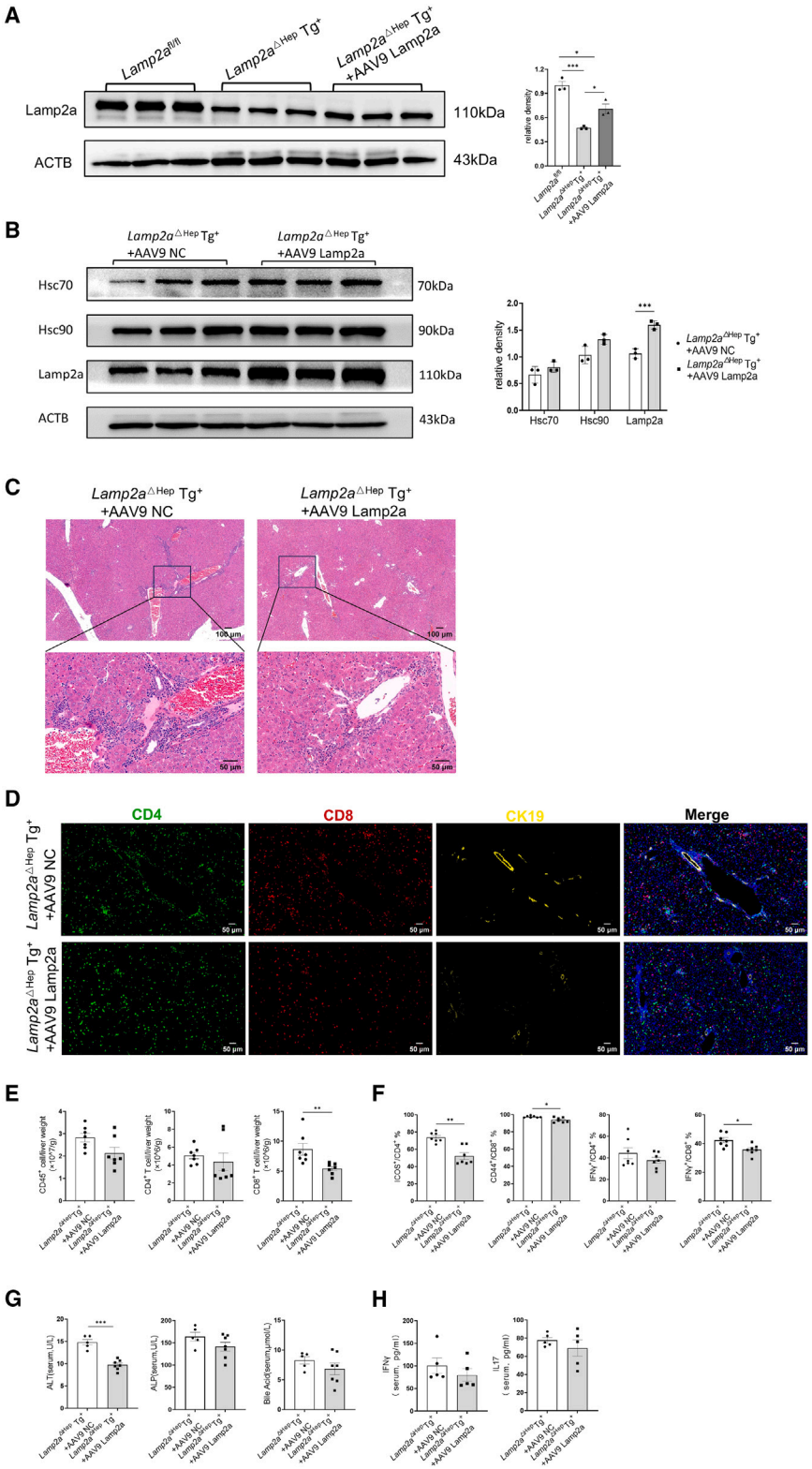


**Figure 2. Hepatic re-expression of Lamp2a alleviates *Lamp2a*$^{\Delta Hep}$ Tg$^+$ mice liver inflammation**

(A) Immunoblot for Lamp2a in liver homogenates from *Lamp2a*$^{fl/fl}$, *Lamp2a*$^{\Delta Hep}$ Tg$^+$ and *Lamp2a*$^{\Delta Hep}$ Tg$^+$+AAV9 Lamp2a mice. ($n$ = 3 mice per groups; *, $p < 0.05$; ***, $p < 0.005$).

(B) Immunoblot for Lamp2a, Hsc70, and Hsc90 in liver homogenates from *Lamp2a*$^{\Delta Hep}$ Tg$^+$ mice treated with AAV9 NC or AAV9 Lamp2a. ($n$ = 3 mice per groups; ***, $p < 0.005$).

(C) H&E staining of liver section from mice described in (A). (scale bar labeled in the figure).

(D) CD4(green), CD8(red), and CK19(yellow) IF staining of liver section from mice described in (B). (scale bar labeled in the figure).

(E) Percentages of CD45.2$^+$, CD4$^+$, and CD8$^+$ cells in liver from mice described in (B), as determined by flow cytometry. ($n$ = 7 mice per group; **, $p < 0.01$).

(F) Percentages of the indicated leukocyte subsets in liver of mice described in (B), as determined by flow cytometry. (*, $p < 0.05$; **, $p < 0.01$).

(G) The serum level of indicated biochemical parameters from mice described in (B). (*Lamp2a*$^{\Delta Hep}$ Tg$^+$+AAV9 NC, $n$ = 5; *Lamp2a*$^{\Delta Hep}$ Tg$^+$+AAV9 Lamp2a, $n$ = 7; ***, $p < 0.005$).

(H) IFN-γ and IL17 levels in serum from mice described in (B), determined by ELISA ($n$ = 5 mice per group). Statistical significance was determined by two-tailed unpaired t test. Data are presented as means ± SEM.

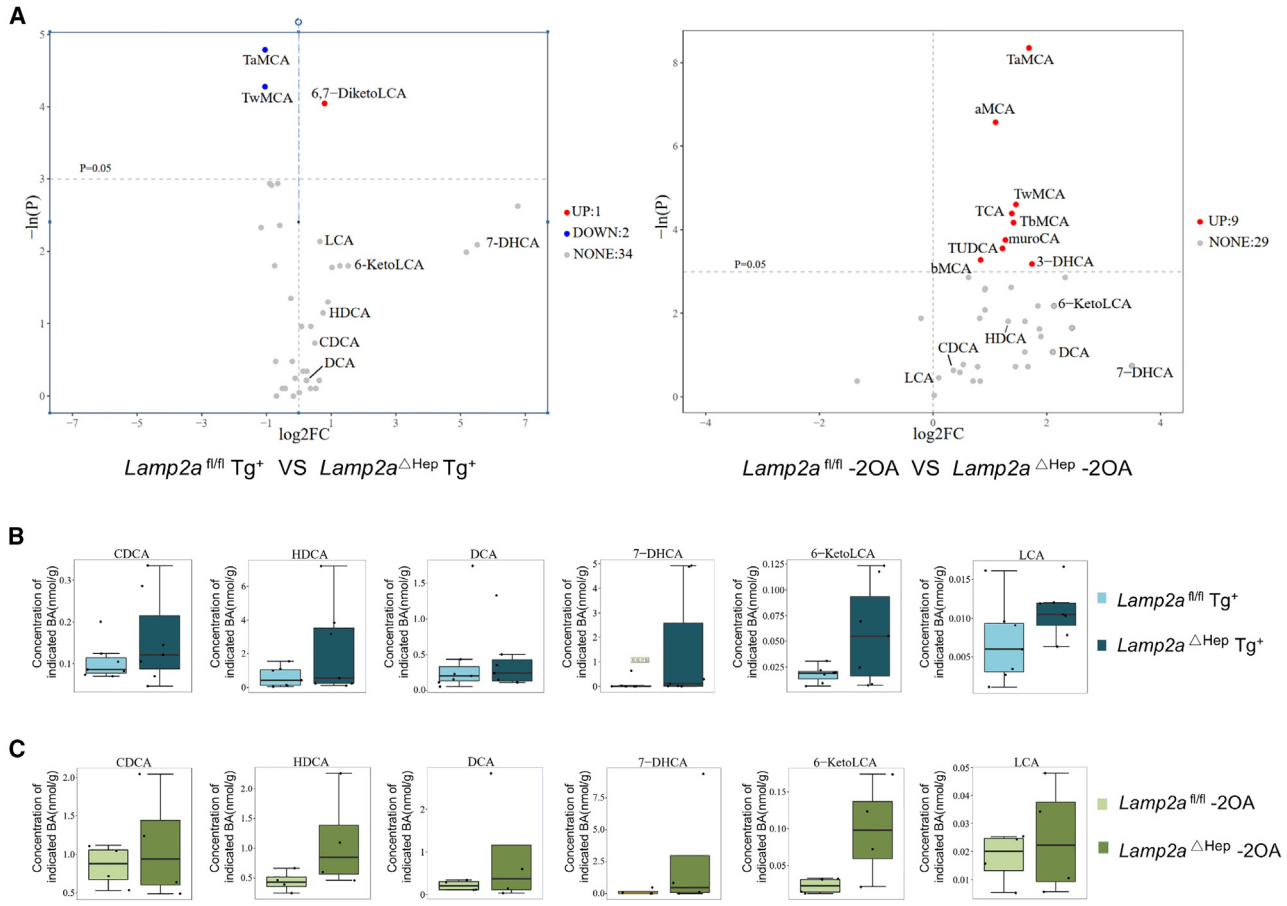


**Figure 3. Bile acid metabolomics in livers of PBC mice model with or without hepatocellular Lamp2a knockout**

(A) Volcano plots of bile acids from livers of *Lamp2a*$^{fl/fl}$Tg$^{+}$ mice VS *Lamp2a*$^{\Delta Hep}$ Tg$^{+}$ mice (left panel) and *Lamp2a*$^{fl/fl}$-2OA mice VS *Lamp2a*$^{\Delta Hep}$ -2OA mice (right panel) (Tg$^{+}$ model, *n* = 7 mice per group; 2OA models *n* = 4 mice per group).

(B) Boxplots of the indicated bile acids from livers of *Lamp2a*$^{\Delta Hep}$ Tg$^{+}$ and *Lamp2a*$^{fl/fl}$Tg$^{+}$ mice(*n* = 7 mice per group).

(C) Boxplots of the indicated bile acids from livers of *Lamp2a*$^{\Delta Hep}$ -2OA and *Lamp2a*$^{fl/fl}$-2OA mice(*n* = 4 mice per group).

did not show significant differences (Figures S6A and S6B), confirmed by qPCR (Figure S6C). The pentapeptide motif of KFERQ was included in the amino acid sequence of Acot8 (Figure S6D), suggesting that Acot8 may be degraded through the CMA pathway. The western blotting analyses revealed that the protein levels of bile acid-metabolizing enzyme, Acot8 were increased after Lamp2a deletion both in mice and cell culture (Figures 4A, 4B, S7A, and S7B) while no significant changes were detected in protein levels of Cyp7a1 and Cyp7b1, another 2 important enzymes of the bile acid synthesis pathway (Figure S7C). Accordingly, the rescue of Lamp2a reduced the levels of Acot8 (Figure S7D). Cytochrome P450 family 27 subfamily A member 1 (Cyp27a1), the rate-limiting enzyme in the alternative pathway of bile acid synthesis, has been reported as substrates of the CMA pathway,[40] prompting that Acot8 might be also degraded via CMA pathway. To test this theory, we observed the degradation of Acot8 in HepG2 and HepG2-L2A cells treated with the protein synthesis inhibitor cycloheximide (CHX). The degradation of Acot8 and Cyp27a1 were significantly slower in HepG2-L2A cells compared to the control group (Figure 4C). Moreover, we found Acot8 and Cyp27a1 were both enriched in the lysosomes of the liver tissue, HepG2 cells and hepatocytes (Figures 4D, 4E, and S7E), and the treatment of the lysosomal inhibitor leupeptin caused their protein accumulation both *in vivo* and *in vitro* (Figures 4F and 4G), while leupeptin had no obvious effect on Cyp27a1 and Acot8 content in the lysosomes of *Lamp2a*$^{\Delta Hep}$ liver and HepG2-L2A (Figures 4F and 4G). The results of the Co-Immunoprecipitation (co-IP) experiments with anti-Lamp2a antibodies showed that both Acot8 and Cyp27a1 could bind to Lamp2a (Figure 4H). Additionally, these two enzymes also have exhibited significant co-localization with Lamp2a in the subcellular structure (Figure 4I). Altogether, these results suggest that the bile acid-metabolizing enzyme Acot8 are degraded via CMA pathway mediated by Lamp2a.

## Knockdown of Acot8 alleviated inflammatory infiltration in the liver

To confirm that Acot8 is an essential linkage during the process of Lamp2a affecting hepatic inflammatory response, we injected *Lamp2a*$^{\Delta Hep}$ Tg$^{+}$ mice with knockdown virus of Acot8 and its

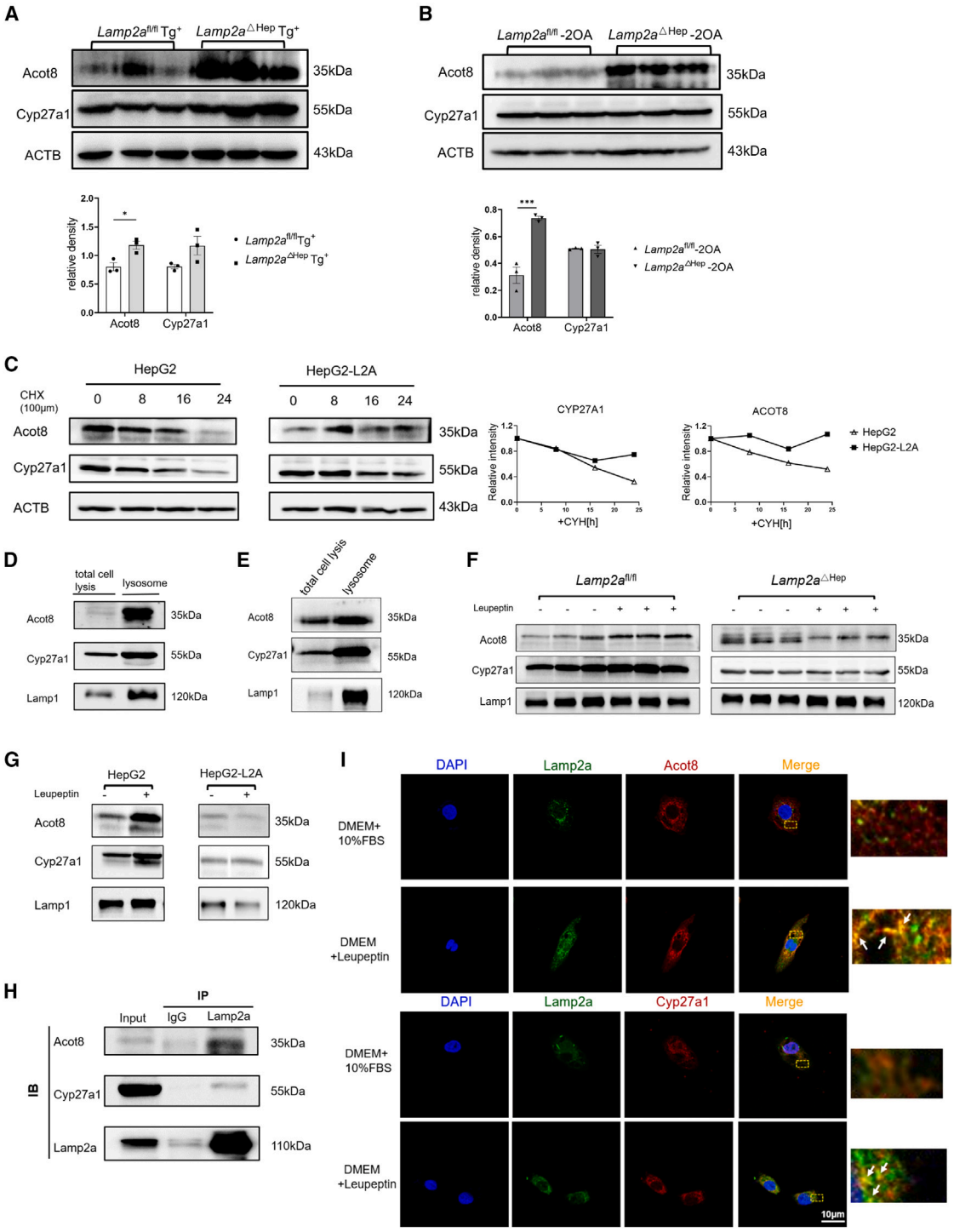


**Figure 4. Mechanisms of regulation of Cyp27a1 and Acot8 by CMA in PBC mice models and HepG2 cell line**

(A and B) Immunoblot showed protein levels of Cyp27a1 and Acot8 in livers from *Lamp2a*$^{fl/fl}$Tg$^{+}$ and *Lamp2a*$^{\Delta Hep}$ Tg$^{+}$ mice (A) or *Lamp2a*$^{fl/f}$-2OA and *Lamp2a*$^{\Delta Hep}$ -2OA (B) mice. ($n$ = 3 mice per groups; *, $p < 0.05$; ***, $p < 0.005$).

(C) Cyp27a1 and Acot8 protein levels in HepG2 and HepG2-L2A cell lines treated with CHX up to 24 h, determined by western blot.

(D and E) Immunoblot showed the enrichment of Cyp27a1 and Acot8 in lysosomal fractions isolated from liver of *Lamp2a*$^{fl/fl}$ mice (D) or HepG2 cells (E) compared to total cell lysis (D, $n$ = 3 mice per group).

(F and G) Cyp27a1 and Acot8 protein levels in lysosomal fractions obtained from livers of *Lamp2a*$^{fl/fl}$ and *Lamp2a*$^{\Delta Hep}$ mice (F) or HepG2 and HepG2-L2A cells (G) treated with or without leupeptin (F, $n$ = 3 mice per group).

*(legend continued on next page)*

control virus to observe its effect on hepatic inflammation. The results showed that knockdown of Acot8 in *Lamp2a*$^{\Delta Hep}$ Tg$^{+}$ mice could significantly reduce the inflammatory infiltration in the liver (Figures 5A–5D). Moreover, the overall immune cell number and CD8$^{+}$ T cell number were both significantly decreased (Figure 5E). Meanwhile, the activation of CD4$^{+}$ T cells and cytotoxic CD8$^{+}$ T cells were also significantly diminished (Figure 5F). Besides, the bile acids HDCA and CDCA, elevated by Lamp2a deletion, showed a decrease following Acot8 knockdown (Figure 5G). The data reported here indicated that knockdown of Acot8 alleviated inflammatory infiltration in the liver.

### Altered bile acid components affect the activity of T lymphocytes

As mentioned earlier, Lamp2a deficiency leads to increased levels of bile acid-metabolism enzymes, which causes alteration in bile acid components. The role played by these altered bile acids in the inflammatory response requires further investigation. To study their effect on T lymphocytes, stimulated T cells were treated with different concentrations of bile acids and examined the proliferation and activation of T cells. The six elevated bile acids mentioned earlier (Figures 3B and 3C) did not affect the proliferation of CD4$^{+}$ and CD8$^{+}$ T cells (Figures S8A and S8B). Importantly, four of the six bile acids could enhance the percentage of IFN-$\gamma^{+}$ in CD4$^{+}$ T cells (Figures 6A and S8C), and three of them, CDCA, DCA, and 7-DHCA, could increase the level of IFN-$\gamma^{+}$ in CD8$^{+}$ T cells (Figures 6B and S8C). Additionally, the activation of CD4$^{+}$ T cells were significantly elevated upon the stimulation by DCA, 6-KetoLCA, and LCA, and that of CD8$^{+}$ T cells did not show obvious change (Figures 6C and 6D). The results here and aforementioned suggested these bile acids, especially CDCA and HDCA, may be effectors of Lamp2a deficiency aggravating hepatic inflammation in murine autoimmune cholangitis.

## DISCUSSION

As a typical autoimmune disease, PBC does not respond to treatment with immunosuppressants, making the development mechanism of this disease elusive. Data reported here suggested us to propose a novel model of CMA mediator Lamp2a during murine autoimmune cholangitis progression (Figure 7). During the disease development in mice, the altered hepatic-Lamp2a level caused the disorder of CMA, leading to abnormal accumulation of enzymes involved in bile acid metabolism and thus causing changes in bile acid components. These altered bile acid components aggravate the inflammatory response by enhancing T lymphocyte activation, thereby promoting the progression of murine autoimmune response. Our study focused on the molecular mechanisms of Lamp2a involved in PBC disease progression, providing a theoretical and experimental basis for the development of novel therapeutic targets for PBC treatment.

To date, the pathogenesis of PBC is unknown, including genetic and environmental factors (intrinsic and extrinsic). There established several mouse models that develop autoimmune cholangitis simulating PBC in a spontaneous or xenobiotic-induced manner. Although none of these mouse models can fully recapitulate all the disease features of human PBC, different models have their unique characteristics and thus are suitable for different studies. The widely used dnTGF-βRII mouse model has been further modified: adoptive transfer of CD8$^{+}$ T cells, B cell deficient (Igμ$^{-/-}$) and IL-2Rα$^{-/-}$ mouse, to study the effects of CD8$^{+}$ T cells, B cells, and liver fibrosis on disease progression respectively.[41–44] Transforming growth factor-β (TGF-β) signal pathway is important for Th17 differentiation. Mutation of TGF-βRII makes it impossible to study Th17 in this model. 2-OA (2-octynoic acid) is a compound mimics fatty acid-lysine synthesis in the domain of PDC-E2. It has been widely used to study the relationship between the onset of PBC and environmental factors. They are disease models based on different triggers respectively (intrinsic and extrinsic). Here, we combined dnTGF-βRII model with the CMA disorder mouse model (*Lamp2a*$^{\Delta Hep}$) to explore the role of Lamp2a during the disease process. Meanwhile, the phenotype of *Lamp2a*$^{\Delta Hep}$ mice immunized with 2-OA led us to further confirm the role of Lamp2a in PBC progression. Although the levels of Lamp2a in the different animal models showed different trends, our results showed Lamp2a deficiency of hepatocytes led to exacerbation of autoimmune cholangitis in the two models.

By comparing the changes of enzyme involved in bile acid metabolism before and after Lamp2a knockdown, we identified Acot8 and Cyp27a1 as substrates of the CMA pathway mediated by Lamp2a, which are key nodes linking the autophagy disorders with altered bile acid components. Bile acid synthesis in the liver includes two pathways: the classical pathway and the alternative pathway, catalyzed by up to 17 enzymes. Cyp27a1, reported as CMA substrate, is the rate-limiting enzyme in the alternative pathway, also participates in the catalytic reactions in the classical pathway. On the other hand, Acot8 is also involved in the downstream reactions of different synthesis pathways of primary bile acids. Afterward, the primary bile acids formed in the liver are transported to the intestine, forming the secondary bile acids in the action of the gut microbiota. Thus, there is no one-to-one correspondence between bile acid-metabolism enzymes and the eventually formed bile acids. The knockdown of Acot8 has reduced the inflammatory infiltration in the liver of Lamp2a knockout autoimmune cholangitis mouse. The result here indicates that the change in liver inflammation caused by the loss of Lamp2a is mediated by the bile acid metabolic enzyme Acot8, which might be a novel target for PBC treatment. Moreover, some of the bile acids that identified in this study are generated by the gut microbiota. The mechanisms of bile acid composition altered caused by Lamp2a deficiency may also involve changes in the components and function of the gut microbiota,

(H) Co-IP of Lamp2a with the indicated proteins (marked on the left) of livers of *Lamp2a*$^{fl/fl}$ mice. Control IgG and input protein are shown as the controls ($n$ = 3 mice).

(I) Lamp2a (green) with Acot8 (red particles) or Cyp27a1(red particles) IF staining of in HepG2 cell line with or without starvation and leupeptin (Scale bar labeled in the figure). Framed areas are enlarged and shown in separate panels, and arrows represent co-localization. Statistical significance was determined by two-tailed unpaired t test. Data are presented as means ± SEM.

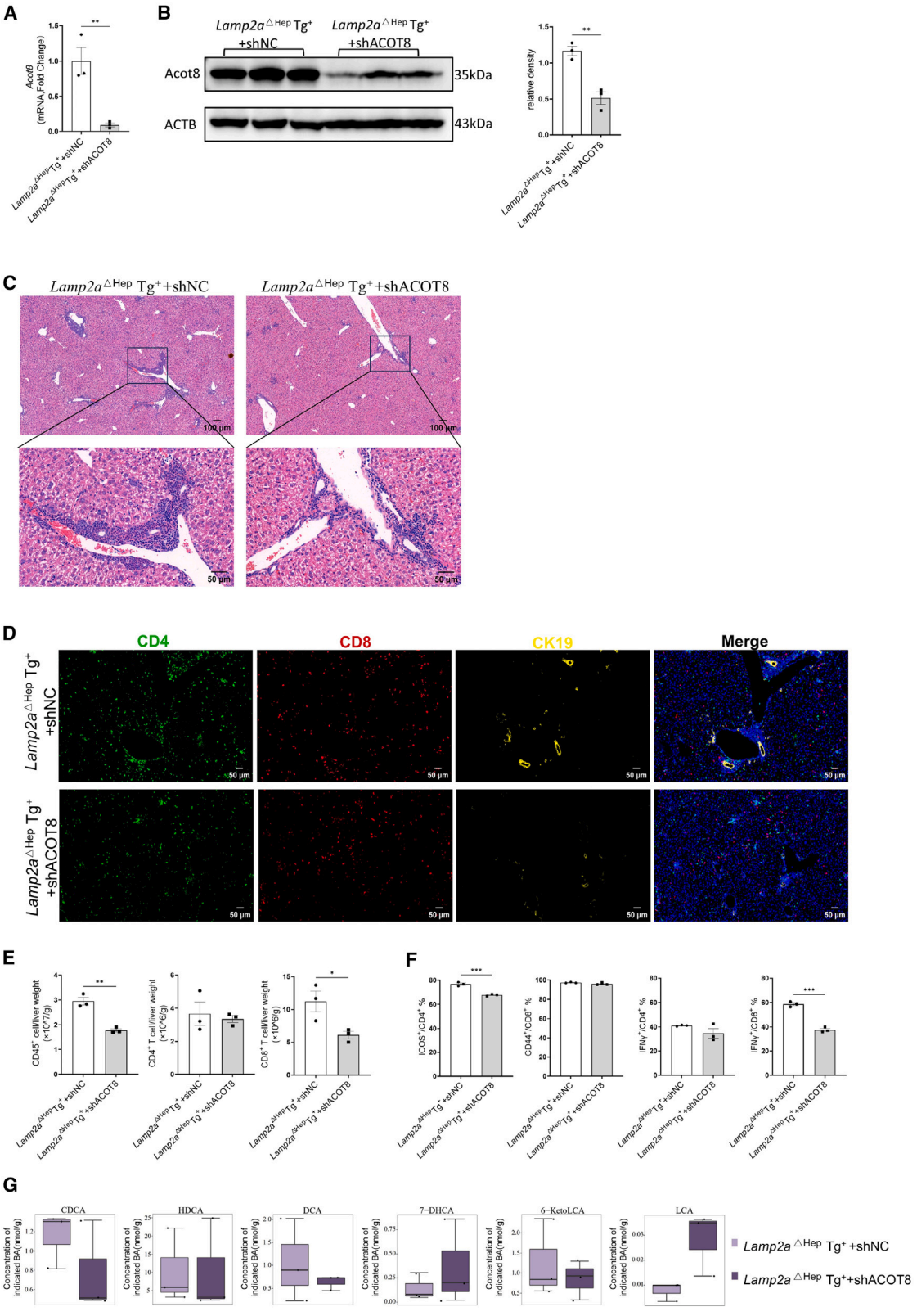


*(legend on next page)*

which is also one of our subsequent research directions. As a signaling molecule, bile acids need to function through the corresponding receptors. There are two known classes of bile acid receptors: one is nuclear receptors including farnesoid X receptor (FXR), vitamin D receptor (VDR), pregnane X receptor (PXR), and constitutive androstane receptor (CAR); the other is membrane receptors, G protein-coupled receptor 5 (TGR5) and sphingosine-1-phosphate receptor 2 (S1PR2). The most studied are FXR and TGR5, involved in the regulation of bile acid metabolism as well as host glycolipids and immunometabolism.[45–48] Whether the stimulatory effect of bile acids on $CD4^+$ and $CD8^+$ T cells observed in this study is directly responsive by T cells to bile acids or exercised indirectly by other cells remains unclear. Either the receptor involved in the direct response or the indirectly mediated cell type requires further exploration. How the absence of Lamp2a changes the components of bile acid metabolism and the effect of bile acid alteration on T cell proliferation and activation will be further explored in subsequent studies.

In conclusion, this study indicated that the deficiency of Lamp2a altered the bile acid components by affecting the levels of key enzymes in bile acid metabolism, which promotes the activity of $CD4^+$ and $CD8^+$ T cells and ultimately participates in the disease progression of murine autoimmune cholangitis, providing the theoretical and experimental basis for PBC intervention and the discovery of new targets.

### Limitations of the study

In this study, we found that the absence of Lamp2a leads to abnormal accumulation of the bile acid metabolism enzyme Acot8, causing changes in the bile acid component and triggering an immune response thus resulting aggravation of liver inflammation. Due to the limitations of the current research method, the various mouse models of PBC are the simulation of disease symptoms rather than disease mechanisms, therefore the findings reported here need to be further verified in clinical samples, which will be conducted in subsequent studies.

## RESOURCE AVAILABILITY

### Lead contact

Further information and requests for resources and reagents should be directed to and will be fulfilled by the lead contact, Ying Han (hanying1@fmmu.edu.cn).

### Materials availability

This study did not generate new unique reagents. All materials in this study are commercially available.

### Data and code availability

- All data reported in this paper will be shared by lead contact upon request.
- The RNA-seq data have been deposited at the National Center for Biotechnology Information's Sequence Read Archive and are publicly available as of the date of publication. Accession numbers are listed in the key resources table.
- This paper does not report original code.
- Any additional information required to reanalyze the data reported in this paper is available from the lead contact upon request.

## ACKNOWLEDGMENTS

We thank Professor Gershwin ME in the University of California at Davis for donating dnTGFβRII model mice. This work was financially supported by National Natural Science Foundation of China (no. 82270551, 81820108005, 82303155, and 82200637) and Key Research and Development Program of Shaanxi (no. 2021ZDLSF02-07, 2022ZDLSF03-03, and 2023KJXX-026).

## AUTHOR CONTRIBUTIONS

Y.Han, T.L., and J.W. conceived and designed the research. Q.F. and G.G. performed most of the experiment and analyzed the data. Y.Hu, Y.L., J.Y., R.S., and E.X. assisted with the experiments and data collection. S.M. and M.Z. provided academic advice. T.L. and Q.F. wrote the manuscript. All authors discussed and edited the manuscript.

## DECLARATION OF INTERESTS

The authors declare no competing interests.

## STAR★METHODS

Detailed methods are provided in the online version of this paper and include the following:

- KEY RESOURCES TABLE
- EXPERIMENTAL MODEL AND STUDY PARTICIPANT DETAILS
  - Animal models
  - Cell lines
- METHOD DETAILS
  - Induction of murine cholangitis by 2OA immunization
  - Adeno-associated virus infection
  - Extraction of primary hepatocytes
  - Extraction of primary liver immune cells
  - Cell treatments
  - Histology and electron microscopy
  - RT-PCR and RNA-seq
  - Western blot
  - Flow Cytometry
  - Quantitative analysis of BAs
  - Coimmunoprecipitation
  - Immunofluorescence co-localization

**Figure 5. Hepatic knockdown of Acot8 alleviates *Lamp2a*$^{\Delta Hep}$ $Tg^+$ mice liver inflammation**

(A and B) Relative mRNA (A) and protein (B) levels of Acot8 in *Lamp2a*$^{\Delta Hep}$ $Tg^+$ +shAcot8 mice compared to *Lamp2a*$^{\Delta Hep}$ $Tg^+$ +shNC group, determined by real-time RT-PCR (A) and western blot (B). ($n = 3$ mice per groups; **, $p < 0.01$).

(C) H&E staining of liver section from mice described in a. (scale bar labeled in the figure).

(D) CD4(green), CD8(red) and CK19(yellow) IF staining of liver section from mice described in (A). (scale bar labeled in the figure).

(E) Percentages of $CD45.2^+$, $CD4^+$, and $CD8^+$ cells in livers from mice described in (A), as determined by flow cytometry.
(*, $p < 0.05$; **, $p < 0.01$).

(F) Percentages of the indicated leukocyte subsets in livers of mice described in (A), as determined by flow cytometry.
(***, $p < 0.005$).

(G) Boxplots of the indicated bile acids from livers of mice described in (A). Statistical significance was determined by two-tailed unpaired t test. Data are presented as means ± SEM.

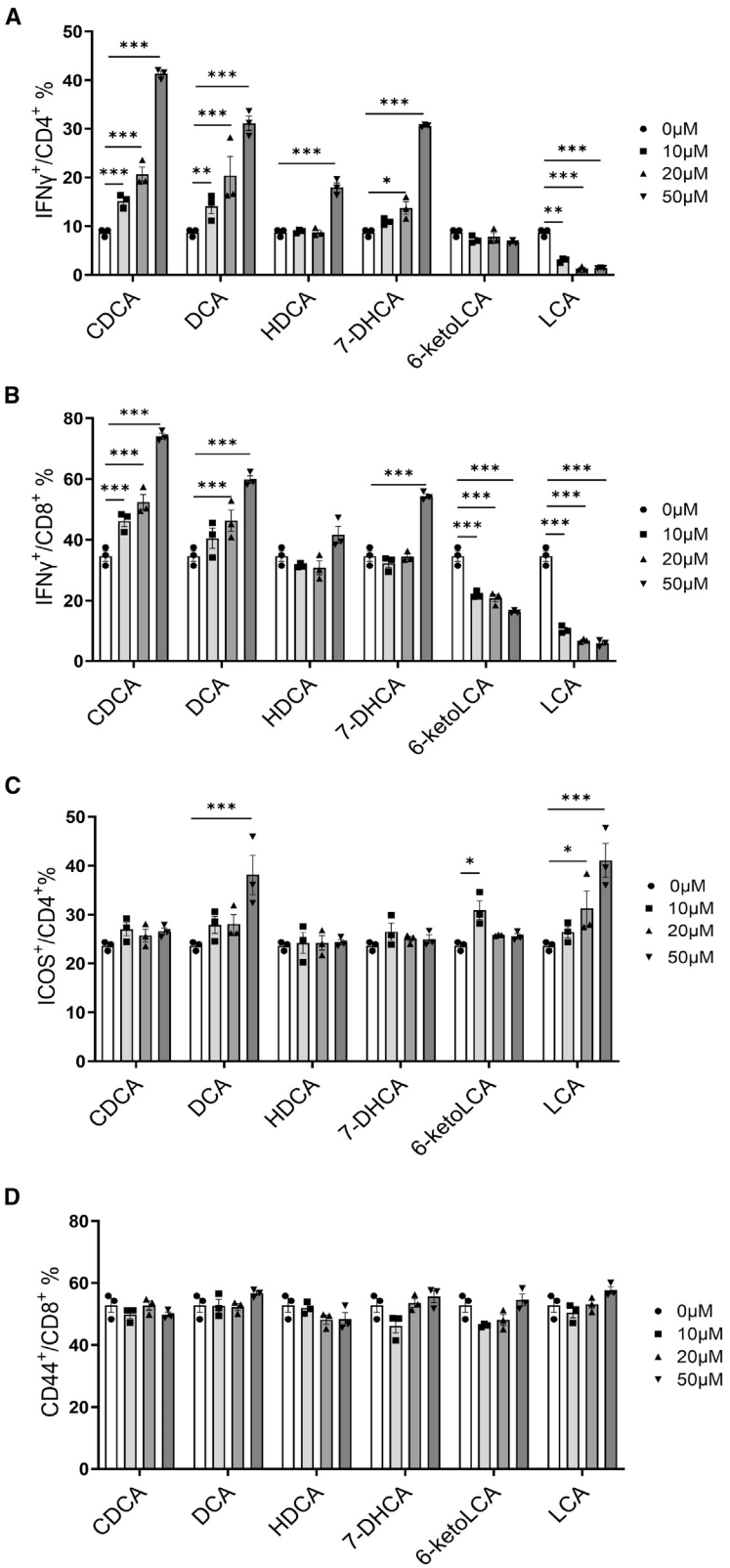


**Figure 6. Effects of CMA-deficient related bile acids on T cell activation**

(A and B) IFN-γ production of $CD4^+$ (A) and $CD8^+$ (B) T cells treated with different concentrations of indicated bile acids determined by flow cytometry.

(*, $p < 0.05$; **, $p < 0.01$; ***, $p < 0.005$).

(C and D) The degree of activated $CD4^+$ (C) and $CD8^+$ (D) T cells treated with different concentrations of indicated bile acids determined by flow cytometry.

(*, $p < 0.05$; ***, $p < 0.005$). Statistical significance was determined by one-way ANOVA with Turkey post-hoc test. For all panels, data are presented as means ± SEM, and are representative of 2 independent experiments.

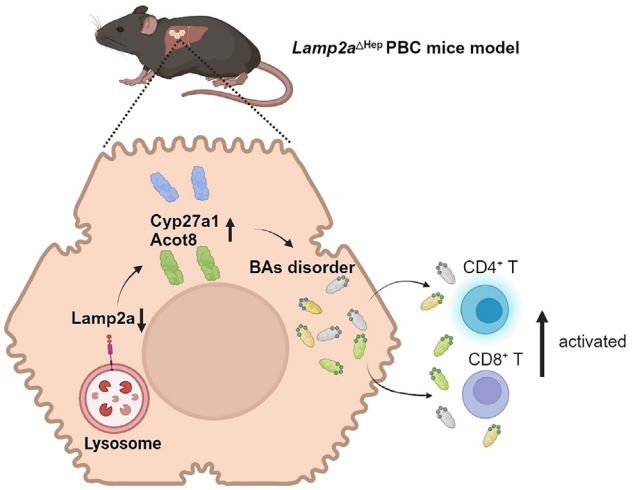


**Figure 7. A working model for the role of hepatic Lamp2a during PBC progression**

- *In vitro* T Cell culture
- ELISA

- QUANTIFICATION AND STATISTICAL ANALYSIS

## SUPPLEMENTAL INFORMATION

Supplemental information can be found online at https://doi.org/10.1016/j.isci.2025.111804.

Received: June 16, 2024
Revised: October 4, 2024
Accepted: January 10, 2025
Published: January 16, 2025

## REFERENCES

1. Jayant, A., and Talwalkar, K.D.L. (2003). Primary biliary cirrhosis. Lancet *362*, 53–61. https://doi.org/10.1016/S0140-6736(03)13808-1.
2. You, H., Ma, X., Efe, C., Wang, G., Jeong, S.H., Abe, K., Duan, W., Chen, S., Kong, Y., Zhang, D., et al. (2022). APASL clinical practice guidance: the diagnosis and management of patients with primary biliary cholangitis. Hepatol. Int. *16*, 1–23. https://doi.org/10.1007/s12072-021-10276-6.
3. Smets, L., Verbeek, J., Korf, H., van der Merwe, S., and Nevens, F. (2021). Improved Markers of Cholestatic Liver Injury in Patients With Primary Biliary Cholangitis Treated With Obeticholic Acid and Bezafibrate. Hepatology *73*, 2598–2600. https://doi.org/10.1002/hep.31613.
4. Gerussi, A., Bernasconi, D.P., O'Donnell, S.E., Lammers, W.J., Van Buuren, H., Hirschfield, G., Janssen, H., Corpechot, C., Reig, A., Pares, A., et al. (2021). Measurement of Gamma Glutamyl Transferase to Determine Risk of Liver Transplantation or Death in Patients With Primary Biliary Cholangitis. Clin. Gastroenterol. Hepatol. *19*, 1688–1697.e14. https://doi.org/10.1016/j.cgh.2020.08.006.
5. Kaplan, M.M., and Gershwin, M.E. (2005). Primary biliary cirrhosis. N. Engl. J. Med. *353*, 1261–1273. https://doi.org/10.1056/NEJMra043898.
6. Chiang, J.Y.L., and Ferrell, J.M. (2020). Bile Acid Biology, Pathophysiology, and Therapeutics. Clin. Liver Dis. *15*, 91–94. https://doi.org/10.1002/cld.861.
7. Evangelakos, I., Heeren, J., Verkade, E., and Kuipers, F. (2021). Role of bile acids in inflammatory liver diseases. Semin. Immunopathol. *43*, 577–590. https://doi.org/10.1007/s00281-021-00869-6.
8. Cai, J., Rimal, B., Jiang, C., Chiang, J.Y.L., and Patterson, A.D. (2022). Bile acid metabolism and signaling, the microbiota, and metabolic disease. Pharmacol. Ther. *237*, 108238. https://doi.org/10.1016/j.pharmthera.2022.108238.
9. Li, Y., Tang, R., Leung, P.S.C., Gershwin, M.E., and Ma, X. (2017). Bile acids and intestinal microbiota in autoimmune cholestatic liver diseases. Autoimmun. Rev. *16*, 885–896. https://doi.org/10.1016/j.autrev.2017.07.002.
10. Chiang, J.Y.L. (2017). Bile acid metabolism and signaling in liver disease and therapy. Liver Res. *1*, 3–9. https://doi.org/10.1016/j.livres.2017.05.001.
11. Schaap, F.G., Trauner, M., and Jansen, P.L.M. (2014). Bile acid receptors as targets for drug development. Nat. Rev. Gastroenterol. Hepatol. *11*, 55–67. https://doi.org/10.1038/nrgastro.2013.151.
12. Poupon, R. (2012). Ursodeoxycholic acid and bile-acid mimetics as therapeutic agents for cholestatic liver diseases: an overview of their mechanisms of action. Clin. Res. Hepatol. Gastroenterol. *36*, S3–S12. https://doi.org/10.1016/S2210-7401(12)70015-3.
13. Ornolfsson, K.T., Lund, S.H., Olafsson, S., Bergmann, O.M., and Bjornsson, E.S. (2019). Biochemical response to ursodeoxycholic acid among PBC patients: a nationwide population-based study. Scand. J. Gastroenterol. *54*, 609–616. https://doi.org/10.1080/00365521.2019.1606931.
14. Kjaergaard, K., Frisch, K., Sørensen, M., Munk, O.L., Hofmann, A.F., Horsager, J., Schacht, A.C., Erickson, M., Shapiro, D., and Keiding, S. (2021). Obeticholic acid improves hepatic bile acid excretion in patients with primary biliary cholangitis. J. Hepatol. *74*, 58–65. https://doi.org/10.1016/j.jhep.2020.07.028.
15. Pedersen, M.R., Greenan, G., Arora, S., Murali, A.R., and Mayo, M.J. (2021). Ursodeoxycholic Acid Decreases Incidence of Primary Biliary Cholangitis and Biliary Complications After Liver Transplantation: A Meta-Analysis. Liver Transpl. *27*, 866–875. https://doi.org/10.1002/lt.25935.
16. Zhao, Y.G., Codogno, P., and Zhang, H. (2021). Machinery, regulation and pathophysiological implications of autophagosome maturation. Nat. Rev. Mol. Cell Biol. *22*, 733–750. https://doi.org/10.1038/s41580-021-00392-4.
17. Boya, P., Reggiori, F., and Codogno, P. (2013). Emerging regulation and functions of autophagy. Nat. Cell Biol. *15*, 713–720. https://doi.org/10.1038/ncb2788.
18. Panzitt, K., Jungwirth, E., Krones, E., Lee, J.M., Pollheimer, M., Thallinger, G.G., Kolb-Lenz, D., Xiao, R., Thorell, A., Trauner, M., et al. (2020). FXR-dependent Rubicon induction impairs autophagy in models of human cholestasis. J. Hepatol. *72*, 1122–1131. https://doi.org/10.1016/j.jhep.2020.01.014.
19. Sasaki, M., Miyakoshi, M., Sato, Y., and Nakanuma, Y. (2013). Increased expression of mitochondrial proteins associated with autophagy in biliary epithelial lesions in primary biliary cirrhosis. Liver Int. *33*, 312–320. https://doi.org/10.1111/liv.12049.
20. Xu, Y., Shen, J., and Ran, Z. (2020). Emerging views of mitophagy in immunity and autoimmune diseases. Autophagy *16*, 3–17. https://doi.org/10.1080/15548627.2019.1603547.
21. Manley, S., Williams, J.A., and Ding, W.X. (2013). Role of p62/SQSTM1 in liver physiology and pathogenesis. Exp. Biol. Med. *238*, 525–538. https://doi.org/10.1177/1535370213489446.
22. Eskelinen, E.L. (2006). Roles of LAMP-1 and LAMP-2 in lysosome biogenesis and autophagy. Mol. Aspects Med. *27*, 495–502. https://doi.org/10.1016/j.mam.2006.08.005.
23. Glick, D., Barth, S., and Macleod, K.F. (2010). Autophagy: cellular and molecular mechanisms. J. Pathol. *221*, 3–12. https://doi.org/10.1002/path.2697.
24. Wang, L., Wang, J., Cai, W., Shi, Y., Zhou, X., Guo, G., Guo, C., Huang, X., Han, Z., Zhang, S., et al. (2017). A Critical Evaluation of Liver Pathology in Humans with Danon Disease and Experimental Correlates in a Rat Model

of LAMP-2 Deficiency. Clin. Rev. Allergy Immunol. *53*, 105–116. https://doi.org/10.1007/s12016-017-8598-3.

25. Wang, L., Guo, G.y., Wang, J.b., Zhou, X.m., Yang, Q., Han, Z.y., Li, Q., Zhang, J.w., Cai, Y., Ren, X.l., et al. (2015). A decline of LAMP- 2 predicts ursodeoxycholic acid response in primary biliary cirrhosis. Sci. Rep. *5*, 9772. https://doi.org/10.1038/srep09772.
26. Wang, L., Wang, J., Shi, Y., Zhou, X., Wang, X., Li, Z., Huang, X., Wang, J., Han, Z., Li, T., et al. (2013). Identification of a primary biliary cirrhosis associated protein as lysosome-associated membrane protein-2. J. Proteomics *91*, 569–579. https://doi.org/10.1016/j.jprot.2013.08.019.
27. Eskelinen, E.L., Cuervo, A.M., Taylor, M.R.G., Nishino, I., Blum, J.S., Dice, J.F., Sandoval, I.V., Lippincott-Schwartz, J., August, J.T., and Saftig, P. (2005). Unifying nomenclature for the isoforms of the lysosomal membrane protein LAMP-2. Traffic *6*, 1058–1061. https://doi.org/10.1111/j.1600-0854.2005.00337.x.
28. Dice, J.F. (2007). Chaperone-mediated autophagy. Autophagy *3*, 295–299. https://doi.org/10.4161/auto.4144.
29. Cuervo, A.M., and Dice, J.F. (2000). Unique properties of lamp2a compared to other lamp2 isoforms. J. Cell Sci. *113*, 4441–4450. https://doi.org/10.1242/jcs.113.24.4441.
30. Qiao, L., Hu, J., Qiu, X., Wang, C., Peng, J., Zhang, C., Zhang, M., Lu, H., and Chen, W. (2023). LAMP2A, LAMP2B and LAMP2C: similar structures, divergent roles. Autophagy *19*, 2837–2852. https://doi.org/10.1080/15548627.2023.2235196.
31. Hasima, N., and Ozpolat, B. (2014). Regulation of autophagy by polyphenolic compounds as a potential therapeutic strategy for cancer. Cell Death Dis. *5*, e1509. https://doi.org/10.1038/cddis.2014.467.
32. Fujiwara, Y., Furuta, A., Kikuchi, H., Aizawa, S., Hatanaka, Y., Konya, C., Uchida, K., Yoshimura, A., Tamai, Y., Wada, K., and Kabuta, T. (2013). Discovery of a novel type of autophagy targeting RNA. Autophagy *9*, 403–409. https://doi.org/10.4161/auto.23002.
33. Zollner, G., Wagner, M., Fickert, P., Silbert, D., Gumhold, J., Zatloukal, K., Denk, H., and Trauner, M. (2007). Expression of bile acid synthesis and detoxification enzymes and the alternative bile acid efflux pump MRP4 in patients with primary biliary cirrhosis. Liver Int. *27*, 920–929. https://doi.org/10.1111/j.1478-3231.2007.01506.x.
34. Sun, K., Ma, S., Tian, S., Zhang, M., Liu, Y., Li, B., Zhou, X., Zheng, X., Zhou, X., Wang, L., and Han, Y. (2021). An enhanced level of LAMP-2A participates in CD4(+)T cell hyperactivity in patients with primary biliary cholangitis. Ann. Transl. Med. *9*, 101. https://doi.org/10.21037/atm-20-2427.
35. Hunt, M.C., Siponen, M.I., and Alexson, S.E.H. (2012). The emerging role of acyl-CoA thioesterases and acyltransferases in regulating peroxisomal lipid metabolism. Biochim. Biophys. Acta *1822*, 1397–1410. https://doi.org/10.1016/j.bbadis.2012.03.009.
36. Tillander, V., Alexson, S.E.H., and Cohen, D.E. (2017). Deactivating Fatty Acids: Acyl-CoA Thioesterase-Mediated Control of Lipid Metabolism. Trends Endocrinol. Metab. *28*, 473–484. https://doi.org/10.1016/j.tem.2017.03.001.
37. Hunt, M.C., and Alexson, S.E.H. (2008). Novel functions of acyl-CoA thioesterases and acyltransferases as auxiliary enzymes in peroxisomal lipid metabolism. Prog. Lipid Res. *47*, 405–421. https://doi.org/10.1016/j.plipres.2008.05.001.
38. Hunt, M.C., Solaas, K., Kase, B.F., and Alexson, S.E.H. (2002). Characterization of an acyl-coA thioesterase that functions as a major regulator of peroxisomal lipid metabolism. J. Biol. Chem. *277*, 1128–1138. https://doi.org/10.1074/jbc.M106458200.
39. Watanabe, H., Shiratori, T., Shoji, H., Miyatake, S., Okazaki, Y., Ikuta, K., Sato, T., and Saito, T. (1997). A novel acyl-CoA thioesterase enhances its enzymatic activity by direct binding with HIV Nef. Biochem. Biophys. Res. Commun. *238*, 234–239. https://doi.org/10.1006/bbrc.1997.7217.
40. Schneider, J.L., Suh, Y., and Cuervo, A.M. (2014). Deficient chaperone-mediated autophagy in liver leads to metabolic dysregulation. Cell Metab. *20*, 417–432. https://doi.org/10.1016/j.cmet.2014.06.009.
41. Yang, G.X., Lian, Z.X., Chuang, Y.H., Moritoki, Y., Lan, R.Y., Wakabayashi, K., Ansari, A.A., Flavell, R.A., Ridgway, W.M., Coppel, R.L., et al. (2008). Adoptive transfer of CD8(+) T cells from transforming growth factor beta receptor type II (dominant negative form) induces autoimmune cholangitis in mice. Hepatology *47*, 1974–1982. https://doi.org/10.1002/hep.22226.
42. Moritoki, Y., Zhang, W., Tsuneyama, K., Yoshida, K., Wakabayashi, K., Yang, G.X., Bowlus, C., Ridgway, W.M., Ueno, Y., Ansari, A.A., et al. (2009). B cells suppress the inflammatory response in a mouse model of primary biliary cirrhosis. Gastroenterology *136*, 1037–1047. https://doi.org/10.1053/j.gastro.2008.11.035.
43. Lin, X., Wang, X., Xiao, F., Ma, K., Liu, L., Wang, X., Xu, D., Wang, F., Shi, X., Liu, D., et al. (2019). IL-10-producing regulatory B cells restrain the T follicular helper cell response in primary Sjogren's syndrome. Cell. Mol. Immunol. *16*, 921–931. https://doi.org/10.1038/s41423-019-0227-z.
44. Yao, Y., Yang, W., Yang, Y.Q., Ma, H.D., Lu, F.T., Li, L., Tao, Y.Y., Tsuneyama, K., Zhang, W., Friedman, S., et al. (2014). Distinct from its canonical effects, deletion of IL-12p40 induces cholangitis and fibrosis in interleukin-2Ralpha(-/-) mice. J. Autoimmun. *51*, 99–108. https://doi.org/10.1016/j.jaut.2014.02.009.
45. Lefebvre, P., Cariou, B., Lien, F., Kuipers, F., and Staels, B. (2009). Role of bile acids and bile acid receptors in metabolic regulation. Physiol. Rev. *89*, 147–191. https://doi.org/10.1152/physrev.00010.2008.
46. Sayin, S.I., Wahlström, A., Felin, J., Jäntti, S., Marschall, H.U., Bamberg, K., Angelin, B., Hyötyläinen, T., Orešič, M., and Bäckhed, F. (2013). Gut microbiota regulates bile acid metabolism by reducing the levels of tauro-beta-muricholic acid, a naturally occurring FXR antagonist. Cell Metab. *17*, 225–235. https://doi.org/10.1016/j.cmet.2013.01.003.
47. Duboc, H., Taché, Y., and Hofmann, A.F. (2014). The bile acid TGR5 membrane receptor: from basic research to clinical application. Dig. Liver Dis. *46*, 302–312. https://doi.org/10.1016/j.dld.2013.10.021.
48. Thomas, C., Gioiello, A., Noriega, L., Strehle, A., Oury, J., Rizzo, G., Macchiarulo, A., Yamamoto, H., Mataki, C., Pruzanski, M., et al. (2009). TGR5-mediated bile acid sensing controls glucose homeostasis. Cell Metab. *10*, 167–177. https://doi.org/10.1016/j.cmet.2009.08.001.

## STAR★METHODS

### KEY RESOURCES TABLE

| REAGENT or RESOURCE | SOURCE | IDENTIFIER |
|---|---|---|
| Antibodies | | |
| Anti-LAMP2A | Abcam | Cat#ab125068; RRID:AB_10971511 |
| Anti-LAMP2A | Abcam | Cat#ab18528; RRID:AB_775981 |
| Anti-Hsc70 | Abcam | Cat#ab51052; RRID:AB_880538 |
| Anti-Hsc90 | Abcam | Cat#ab203126; RRID:AB_2800428 |
| Anti-β-actin | Proteintech | Cat#20536-1-AP; RRID:AB _10700003 |
| Anti-CD4 | Cell Signaling Technology | Cat#25229; RRID:AB_2798898 |
| Anti-CD8α | Cell Signaling Technology | Cat#98941; RRID:AB_2756376 |
| Anti-CK19 | Abcam | Cat#ab52625; RRIDAB_2281020 |
| Anti-LAMP1 | Abcam | Cat#ab208943; RRID:AB_2923327 |
| Anti-LAMP1 | Abcam | Cat#ab108597; RRID:AB_2915985 |
| Anti-CYP27A1 | Abcam | Cat#ab126785; RRID:AB_11128459 |
| Anti-CYP27A1 | Santa Cruz | Cat#sc-390974; RRID:AB_2261410 |
| Anti-Acot8 | Santa Cruz | Cat#sc-7343; RRID:AB_2221665 |
| Anti-Acot8 | GeneTex | Cat#GTX103960;RRID:AB_1949568 |
| Anti-CYP7B1 | Proteintech | Cat#24889-1-AP; RRID :AB_2879780 |
| Anti-CYP7A1 | GeneTex | Cat# GTX108871; RRID:AB_2036732 |
| IPKine™ HRP, Mouse Anti-Rabbit IgG LCS | Abbkine | Cat#A25022; RRID:AB_2893334 |
| Goat anti-Rabbit IgG (H+L) Highly Cross-Adsorbed Secondary Antibody, Alexa Fluor™ 488 | Invitrogen | Cat#A-11034;RRID: AB_2576217 |
| Goat anti-Mouse IgG (H+L) Cross-Adsorbed Secondary Antibody, Alexa Fluor™ 594 | Invitrogen | Cat#A11005; RRID:AB_2534073 |
| HRP-conjugated Goat Anti-Rabbit IgG(H+L) | Proteintech | Cat#SA00001-2; RRID:AB_2722564 |
| HRP-conjugated Goat Anti-Mouse IgG(H+L) | Proteintech | Cat#SA00001-1; RRID:AB_2722565 |
| CD3e Monoclonal Antibody (145-2C11) | Invitrogen | Cat#16-0031-85; RRID:AB_468848 |
| Purified anti-mouse CD28 Antibody | Biolegend | Cat#102102; RRID:AB_312867 |
| APC/Cyanine7 anti-mouse CD45.2 Antibody | Biolegend | Cat#109824; RRID:AB_830789 |
| FITC anti-mouse/human CD11b Antibody | Biolegend | Cat#101206; RRID:AB_312789 |
| PE anti-mouse F4/80 Antibody | Biolegend | Cat#123110; RRID:AB_893486 |
| Brilliant Violet 421™ anti-mouse CD3ε Antibody | Biolegend | Cat#100336; RRID:AB_11203705 |
| FITC anti-mouse CD4 Antibody | Biolegend | Cat#100510; RRID:AB_312713 |
| FITC anti-mouse CD3ε Antibody | Biolegend | Cat#100306; RRID:AB_312671 |

(*Continued on next page*)

*Continued*

| REAGENT or RESOURCE | SOURCE | IDENTIFIER |
|---|---|---|
| PerCP/Cyanine5.5 anti-mouse CD4 Antibody | Biolegend | Cat#100540; RRID:AB_893326 |
| APC anti-mouse CD8a Antibody | Biolegend | Cat#100712; RRID:AB_312751 |
| PerCP anti-mouse/human CD44 Antibody | Biolegend | Cat#103036; RRID:AB_10645506 |
| PE anti-human/mouse/rat CD278 (ICOS) Antibody | Biolegend | Cat#313508; RRID:AB_416332 |
| PE anti-mouse IFN-γ Antibody | Biolegend | Cat#163504; RRID:AB_2890730 |
| Brilliant Violet 421TM anti-mouse IL17A | Biolegend | Cat#506926; RRID:AB_2632611 |
| APC/Cyanine7 anti-mouse CD8a Antibody | Biolegend | Cat#100714; RRID:AB_312753 |
| PE/Cyanine7 anti-mouse CD4 Antibody | Biolegend | Cat#100422; RRID:AB_312707 |
| HRP-labeled Goat Anti-Rabbit IgG (H+L) | Servicebio | Cat#GB23303; RRID:AB_2811189 |
| **Bacterial and virus strains** | | |
| AAV9-Lamp2a OE | Shanghai Genechem | N/A |
| AAV8-mir30-shACOT8 | Shandong Vigene Biosciences | N/A |
| **Chemicals, peptides, and recombinant proteins** | | |
| ProLong™ Glass Antifade Mountant with NucBlue™ Stain | Invitrogen | Cat#P36985 |
| 2OA-BSA | Xi'an Ruixi | Cat#R-C-1206 |
| Diphtheria Toxin | Sigma | Cat#D0564 |
| Complete Freund's Adjuvant | Sigma | Cat#F5881 |
| Incomplete Freund's Adjuvant | Sigma | Cat#F5506 |
| Poly I:C | invivogen | Cat#tlrl-picw |
| Percoll | cytiva | Cat#17089101 |
| eBioscienceTM Cell Stimulation Cocktail | Invitrogen | Cat#00-4970-03 |
| Leupeptin Hemisulfate | Selleck | Cat#S7380 |
| Cycloheximide | MCE | Cat#HY-12320 |
| Collagenase Type IV | Sigma | Cat#C4-BIOC |
| iF647 fluorescent labeling of tyramine | Servicebio | Cat#G1232 |
| iFCy3 fluorescent labeling of tyramine | Servicebio | Cat#G1223 |
| iF488 fluorescent labeling of tyramine | Servicebio | Cat#G1231 |
| Deoxycholic acid (DCA) | GLPBIO | Cat# GC33762 |
| Lithocholic acid (LCA) | GLPBIO | Cat# GC17057 |
| Chenodeoxycholic acid(CDCA) | GLPBIO | Cat#GC17985 |
| Hyodeoxycholic acid (HDCA) | GLPBIO | Cat#GN10489 |
| Dehydrochholic acid(7-DHCA) | GLPBIO | Cat#GC34003 |
| 6-keto Lithocholic acid 6-KetoLCA | GLPBIO | Cat#GC49429 |
| **Critical commercial assays** | | |
| Animal Total RNA Isolation Kit | FORE GENE | Cat#RE-03014 |
| Mouse IFN-γ ELISA KIT | 4A bio | Cat#CME0003-096 |
| Mouse IL-17A ELISA KIT | 4A bio | Cat#CME0041-096 |
| PureProteomeTMProteinA/GmixMagneticBeads | Millipore | Cat#LSKMAGA10 |
| Zombie Violet™ Fixable Viability Kit | Biolegend | Cat#423114 |

(*Continued on next page*)

*Continued*

| REAGENT or RESOURCE | SOURCE | IDENTIFIER |
|---|---|---|
| Zombie Aqua™ Fixable Viability Kit | Biolegend | Cat#423102 |
| CFSE Cell Division Tracker Kit | Biolegend | Cat#423801 |
| Minute™ Lysosome Isolation Kit for mammalian cells/tissues | Invent | Cat# LY-034 |
| **Deposited data** | | |
| RNA-seq data for liver of dnTGF-βRII mice | This study | Accession number:PRJNA1189879 https://www.ncbi.nlm.nih.gov/ |
| Bile acid metabolomics for liver of PBC models upon different treatments | This study | N/A |
| **Experimental models: Cell lines** | | |
| HepG2 | ATCC | Cat#HB-8065 |
| HepG2-L2A | BIOCYTOGEN | N/A |
| **Experimental models: Organisms/strains** | | |
| ALB-CRE mice | BIOCYTOGEN | Cat#110137 |
| Lamp2a$^{fl/-}$ mice | BIOCYTOGEN | N/A |
| dnTGF-βRII mice | Donated by University of California at Davis | N/A |
| **Oligonucleotides** | | |
| qPCR primers: Actin Forward: CGTTGACATCCGTAAAGACCTCTA Reverse: CATCGTACTCCTGCTTGCTGATC | This study | N/A |
| qPCR primers: Lamp2a Forward: TGTATTTGGCTAATGGCTCAGC Reverse: TATGGGCACAAGGAAGTTGTC | This study | N/A |
| qPCR primers: Cyp27a1 Forward: AAACTCCCGGATCATCACAGAAA Reverse: GATGTAGGATCCCAGGGTTATCA | This study | N/A |
| qPCR primers: Cyp27a1 Forward: AAACTCCCGGATCATCACAGAAA Reverse: GATGTAGGATCCCAGGGTTATCA | This study | N/A |
| qPCR primers: Cyp7a1 Forward: GCAACTAAACAACCTGCCAGTAC Reverse: TCATCAAGGTACCGGTCGTATTT | This study | N/A |
| qPCR primers: Cyp7b1 Forward: GGAGCCACGACCCTAGATG Reverse: TGCCAAGATAAGGAAGCCAAC | This study | N/A |
| qPCR primers: Acot8 Forward: GCTCCTTGGTGCTGGGATTATAG Reverse: GCTCCTGTCCGTATCCTCTCTAC | This study | N/A |
| **Software and algorithms** | | |
| ImageJ | ImageJ | https://imagej.net/Downloads |
| Graphpad Prism 9.0 | Graphpad Prism | https://www.graphpad.com/scientificsoftware/prism |
| FlowJo Software | FlowJo | https://www.flowjo.com/solutions/flowjo/downloads |
| CaseViewer Software | 3DHISTECH | https://www.3dhistech.com/solutions/caseviewer |

## EXPERIMENTAL MODEL AND STUDY PARTICIPANT DETAILS

### Animal models

All animal studies were approved by the Institutional Animal Care and Use Committee of the Fourth Military Medical University in accordance with NIH guidelines (20220462). Mice were housed in a pathogen-free animal facility at 22 ± 2°C under a controlled 12-h light/dark cycle. We generated Lamp2a$^{flox/flox}$ mice by standard CRISPR/Cas9-mediated gene editing strategy. To specifically delete the Lamp2a from hepatocytes, *Lamp2a*$^{flox/flox}$ mice were bred with a hepatocytes-driven Cre transgenic mouse strain (Alb-Cre) to generate the *Lamp2a*$^{\Delta Hep}$ mice on a C57BL/6 background, *Lamp2a*$^{fl/fl}$ littermates were used as controls. dnTGFβRII mice

were initially donated from University of California at Davis, and then transported to the Fourth Military Medical University. *Lamp2a*$^{fl/fl}$ mice, *Lamp2a*$^{\Delta Hep}$ mice and dnTGFβRII mice were crossed to generate *Lamp2a*$^{fl/fl}$ dnTGFβRII mice(*Lamp2a*$^{fl/fl}$Tg$^{+}$ mice) and *Lamp2a*$^{\Delta Hep}$ dnTGFβRII mice(*Lamp2a*$^{\Delta Hep}$ Tg$^{+}$ mice).The female group was sacrificed at 24-weeks-old for research. Liver tissues were collected for histological evaluation, liver lymphocytes population phenotypes were studied by flow cytometry. Blood chemistry and total bile acid were measured using the commercially available kits from Nanjing Jiancheng according to the manufacturer's protocol. Liver lysosomes were isolated from 16 hour-starved *Lamp2a*$^{fl/fl}$ mice and *Lamp2a*$^{\Delta Hep}$ mice (6-8 weeks) treated or not with leupeptin (40mg/kg,i.p.) two hours before isolation. Four different sets of lysosomes were isolated with Minute$^{TM}$ Lysosme Isolation Kit for mammalian cell/tissue (Invent) according to specification.

### Cell lines

The HepG2 cell line was obtained from State Key Laboratory of Cancer Biology. We generated Lamp2a KO HepG2(HepG2-L2A) cell line by standard CRISPR/Cas9-mediated gene editing strategy. The cell lines were cultured in DMEM supplemented with 10% (v/v) FBS (BI) and 1% penicillin/streptomycin. All cells were cultured at 37°C with 5% (v/v) $CO_2$. All the cell lines were tested for mycoplasma contamination.

## METHOD DETAILS

### Induction of murine cholangitis by 2OA immunization

Female *Lamp2a*$^{flox/flox}$ mice and *Lamp2a*$^{\Delta Hep}$ mice at 8 to 10 weeks of age were maintained in ventilated cages under specific pathogen-free (SPF) conditions. In treatment groups (n = 7 per group), each mouse was immunized with a mixture of BSA-conjugate 2-octynoic acid (2OA) (100μg/50μl phosphate-buffered saline (PBS) intraperitoneally in Complete Freund's Adjuvant (50μl; CFA, Sigma-Aldrich) containing 10 mg/ml of Mycobacterium tuberculosis strain H37Ra, and subsequently boosted every 2 weeks with BSA conjugate 2OA in Incomplete Freund's Adjuvant (IFA, Sigma-Aldrich). Additionally, mice received 100 ng of pertussis toxin (Sigma) at the time of 2 days after the initial immunization. Poly I:C (invivogen) was injected intraperitoneally at a dose of 5 mg/kg once every 3 days from the firstimmunization with 2OA-BSA in CFA. As controls, a comparable number of female *Lamp2a*$^{fl/fl}$ mice (n=5) were treated with PBS with the identical dose. Mice were sacrificed at 12 weeks after primary immunization; liver tissues were collected for histological evaluation; livers lymphocytes population phenotypes were studied by flow cytometry.

### Adeno-associated virus infection

To overexpress Lamp2a or knock Acot8 down *in vivo*, we transduced *Lamp2a*$^{\Delta Hep}$ Tg$^{+}$ mice with adeno-associated virus serotype 9 (AAV9) that encoded a green fluorescent protein (GFP) reporter together with GV599 vector targeting Lamp2a (Genechem Co. LTD, Shanghai, China) or adeno-associated virus serotype 8 (AAV8) that encoded mir30shRNA targeting Acot8 (Vigenebio,Shandong,China) via tail vein. Fourteen *Lamp2a*$^{\Delta Hep}$ Tg$^{+}$ (female, 8-week-old) mice were randomly divided into 2 groups (n = 7 per group) as follows: *Lamp2a*$^{\Delta Hep}$ Tg$^{+}$+AAV9 Lamp2a, *Lamp2a*$^{\Delta Hep}$ Tg$^{+}$+AAV9 NC. Six *Lamp2a*$^{\Delta Hep}$ Tg$^{+}$ (female, 8-week-old) mice were randomly divided into 2 groups (n = 3 per group) as follows: *Lamp2a*$^{\Delta Hep}$ Tg$^{+}$+shNC, *Lamp2a*$^{\Delta Hep}$ Tg$^{+}$+shACOT8. At 8 weeks of age, mice were injected different AAV via tail vein respectively. We also overexpressed Lamp2a with adeno-associated virus serotype 9 (AAV9) in *Lamp2a*$^{fl/fl}$Tg$^{+}$ (female, 8-week-old) mice and *Lamp2a*$^{\Delta Hep}$ -2OA mice (female, 8-week-old). Six *Lamp2a*$^{fl/fl}$Tg$^{+}$ mice were randomly divided into 2 groups (n = 3 per group) as follows: *Lamp2a*$^{fl/fl}$Tg$^{+}$+ AAV9 Lamp2a, *Lamp2a*$^{fl/fl}$Tg$^{+}$+ AAV9 NC. Six *Lamp2a*$^{\Delta Hep}$ -2OA mice were also divided into 2 groups (n = 3 per group): *Lamp2a*$^{\Delta Hep}$ -2OA + AAV9 Lamp2a, *Lamp2a*$^{\Delta Hep}$ -2OA + AAV9 NC. The AAV9 virus was injected before 2OA immunization. Mice were sacrificed at 8 or 12 weeks after injection, and blood and liver tissues were collected and stored for further analysis.

### Extraction of primary hepatocytes

The hepatocytes of *Lamp2a*$^{fl/fl}$, *Lamp2a*$^{fl/fl}$Tg$^{+}$ and *Lamp2a*$^{\Delta Hep}$ Tg$^{+}$ (n=3) were extractd by collagenase digestion method. We cannulated the inferior vena cava, perfused liver with liver perfusion medium(Gibco) to remove blood and Collagenase IV(100CDU/ml, sigma) to digest the liver. The hepatocytes were isolated in liver wash medium(Gibco). The cell suspension was purified by 40% Percoll(cytiva) at 4°, 400g, 10min, no brake. We resuspend cell pellets with William's E medium (containing 10% FBS, Gibco) for further experiment.

### Extraction of primary liver immune cells

The liver samples were grinded by mechanical disintegration with DMEM(containing 2% FBS). The cell suspension was contrifuged at 650rpm, 1min, to discard most parenchyma cell. The supernatant was treated at 450g, 5min. Cell sediments were re-suspended by 40%percol and ontrifuged at 850g, 20min.The Single-cell suspension of the liver immune cells were obtained by this density gradient centrifugation.

### Cell treatments

HepG2 and HepG2-L2A cell lines were cultured by DMEM without serum, and treated with or without the lysosomal inhibitors leupeptin (100 μM) for 16h. Then they were collected for lysosome extraction(Minute$^{TM}$ lysosome separation kit, Invent Biotechnologies).

The HepG2 and HepG2-L2A cell lines were also treated with cycloheximide (CHX, MCE), and collected at different time points(0h,6h,16h,24h) for following research.

### Histology and electron microscopy

Histology was performed on paraffin-embedded liver samples, and evaluated by H&E staining, Masson staining and Multiplex Immunohistochemistry(mIHC). Liver sample was cut into 5μm thick sections and mounted onto slides. The sections were deparaffinized and stained with H&E and Masson. mIHC of sections were blocked with normal goat serum (CST) for 1h. Then they were incubated with anti-CD4 antibody (CST, 25229, 1:100) at 4°C overnight. After washed with PBS, the sections were incubated with horseradish peroxidase (HRP)-conjugated secondary antibody for 1 h at room temperature. Then they were incubated with iFCy3-Tyramide(Servicebio,G1232,1:500) for 10min, and performed by citrate repair for antigen retrieval. The CD8(CST,98941,1:400) and CK19 (abcam, ab52625,1:400) staining were performed in sequence. iF488-Tyramide(Servicebio, G1232, 1:500) and iF647-Tyramide(Servicebio, G1232, 1:500) were added to CD8 and CK19 staining respectively. Histopathological images were collected by Digital scanner(3DHISTECH) and laser scanning confocal microscope (FV3000,Olymbus). For electron microscopy, livers were fixed with 2.5% glutaraldehyde in 0.1 M phosphate buffer (pH 7.4), followed by 1% OsO4. The tissues were dehydrated at room temperature, embedded, ultrathin sectioned and stained. Sections were examined with a HT7800 electron microscope (HITACHI). Images were acquired digitally.

### RT-PCR and RNA-seq

Total RNA from mouse liver tissue was prepared with an animal total RNA isolation kit (FORGENE) according to the manufacturer's instructions. Reverse transcription was performed using oligo deoxythymidine primers. The cDNA was amplified with a Bio-Rad CFX96TMsystem. β-actin mRNA was used as an internal control to normalize mRNA expression. RNA-seq was performed by Gene Denovo Biotechnology Co (Guangzhou, China). Briefly, total RNA of liver was extracted using Trizol reagent kit (Invitrogen, Carlsbad, CA, USA) according to the manufacturer's protocol, and mRNA was enriched by Oligo(dT) beads. Then the enriched mRNA was fragmented into short fragments using fragmentation buffer and reverse transcripted into cDNA with random primers. Then the cDNA fragments were purified with QiaQuick PCR extraction kit (Qiagen, Venlo, The Netherlands), end repaired, poly(A) added, and ligated to Illumina sequencing adapters. The ligation products were size selected by agarose gel electrophoresis, PCR amplified, and sequenced using Illumina Novaseq6000.

### Western blot

Protein expression was determined by Western blot analysis. The cells or liver tissues were lysed in radioimmunoprecipitation assay (RIPA) buffer in the presence of protease inhibitor cocktail (MEMD Millipre) and phosphatase inhibitor cocktail (MEMD Millipre). The protein concentration was determined by a BCA kit (Thermo Scientific). Cell lysates were then subjected to 10% SDS–polyacrylamide gel electrophoresis and transferred to nitrocellulose membranes (BioTrace$^{TM}$). The membranes were blocked in 5% nonfat milk and probed overnight at 4°C with primary antibodies, followed by incubation for 1h at room temperature with secondary antibodies. Protein signals were detected by the imaging system (Bio-Rad) using ECL reagent (4A BIOTECH) and quantified by ImageJ software.

### Flow Cytometry

For intracellular staining, single-cell suspension of the liver immune cells were first incubated for 4 h with eBioscience$^{TM}$ Cell Stimulation Cocktail, a mixure of phorbol 12-myristate 13-acetate and ionomycin (Invitrogen, 1:500). The immune cells were collected and resuspended in 100μL of phosphate-buffered saline (PBS), and incubated with surface markers in the dark for at least 30 min. Then they were fixed and permeabilized and stained with intracellular cytokines, IFN-r and IL-17 for 1 hour. Data were acquired by BD Canto II Flow Cytometry and analyzed using the BD FACS Diva software or FlowJo.v10 software (BD, USA).

### Quantitative analysis of BAs

BAs quantification was performed by Metabo-Profile Biotechnology (Shanghai) Co., LTD using UPLC-MS/MS. All the bile acids standards were synthesized by Metabo-Profile lab or obtained from Steraloids Inc. (Newport, RI, USA) and TRC Chemicals (Toronto, ON, Canada). In brief, 10 mg liver tissue was homogenized with 200 μL acetonitrile/methanol (v/v = 80:20) containing 10 μL internal standard. After centrifugation for 20 min at 13500 rpm at 4°C, the supernatant was transferred to 96-well plate and freeze-dried. Then redissolve samples in 100 μL 1:1 mixture solution of acetonitrile/methanol(v/v = 8:2) and ultrapure water, and centrifuge mixtures at 13500 rpm for 20 min at 4°C, supernatants were transferred into a new 96-well plate for UPLC/TQ-MS analysis with a volume of 5 μL. All the samples were run in a randomized order to minimize systematic analytical errors and pooled with quality control samples. The peak annotation and quantification were performed by MassLynx v4.1 and TargetLynx V4.1 (Waters Corp, Milford, MA, USA).

### Coimmunoprecipitation

*Lamp2a*$^{fl/fl}$ mice liver were collected after 16h starvation, washed with PBS and then homogenated in ice-cold IP lysis buffer containing protease inhibitor and phosphatase inhibitor cocktail (MEMD Millipre). After incubation with magnetic beads(Millipore,Sigma) for 2 h at 4°C, anti-Lamp2a(abcam,125068,1:60) or rabbit control IgG antibody(Santa Cruz Biotechnology,1:100) and new magnetic

beads were added and protein extracts were incubated overnight at 4°C. Proteins bound to the beads were collected by magnetic separator, and eluted with 5× SDS loading buffer at 95°C for 10 min, then followed by western blot analysis.

### Immunofluorescence co-localization

HepG2 cells climbing tablets were fixed with 4% paraformaldehyde, permeabilized by 0.1% Triton X-100, blocked by 5% serum and incubated with antibodies against Lamp2a (abcam, 18528,1:100), Cyp27a1(Santa,sc-390974,1:100), Acot8(Santa,sc-7343,1:100) at room temperature for 1h.Then the samples were washed with PBS twice, and incubated with AF$^{TM}$488-conjugated Goat Anti-Rabbit IgG(H+L)(Invitrogen$^{TM}$,1:250) and AF$^{TM}$594-conjugated Goat Anti-Mouse IgG(H+L) (Invitrogen$^{TM}$, 1:250) for 0.5h. The tablets were sealed with ProLong$^{TM}$ Glass Antifade Mountant with NucBlue$^{TM}$ (Invitrogen$^{TM}$, P36985). Images were captured in a laser scanning confocal microscope (FV3000,Olymbus) .

### *In vitro* T Cell culture

Lymphocytes were isolated from the spleens of C57BL/6 mice. The cells were resuspended with 5 μM carboxyfluorescein diacetate succinimidyl ester (CFSE, Biolegend) working fluid and incubated in a carbon dioxide cell incubator for 10 min. After labeled with CFSE, 1-2×10$^5$ cells were cultured in a 96-well U bottom plate with Roswell Park Memorial Institute (RPMI) medium supplemented with 0.1 mM nonessential amino acids, 1 mM sodium pyruvate, 2 mM l-glutamine, 25 mM HEPES, 55μM 2-mercaptoethanol, 10% FCS and 1% penicillin streptomycin. Meanwhile, they were cultured with the addition of anti-CD3 (invitrogen, clone 145–2C11,1:4000) , anti-CD28 (Biolegend, clone 37.51,1:2000) and different concentrations of bile acids for 3 days. For intracellular staining, lymphocytes were incubated with eBioscience$^{TM}$ Cell Stimulation Cocktail for the last 4 h. Then the treated cells were collected for fluorescence-activated cell sorting (FACS) analysis profiled as previously described.

### ELISA

Sera of PBC mice models were collected. IFNγ and IL17 levels were measured in a sandwich ELISA kits (4A BIOTECH) following the manufacturer's instructions.

## QUANTIFICATION AND STATISTICAL ANALYSIS

Statistical analyses were performed using GraphPad Prism 9.0. All data were tested for normality and equal variance. If passed, Student's t test was used to compare two groups or one-way analysis of variance (ANOVA) followed by Tukey post hoc test for comparisons among >2 groups. Otherwise, nonparametric tests (Mann-Whitney U test or Kruskal-Wallis test followed by Dunn's post hoc test) were used. All results were expressed as means ± SEM. P value <0.05 was considered statistically significant.